Research Article | Vol. 8, No. 6 | 1 Jun 2017 | BIOMEDICAL OPTICS EXPRESS 2866
Biomedical Optics EXPRESS

Digital micromirror based near-infrared illumination system for plasmonic photothermal neuromodulation

HYUNJUN JUNG, HONGKI KANG, AND YOONKEY NAM*

Department of Bio and Brain Engineering, Korea Advanced Institute of Science and Technology, Daejeon 34141, South Korea
**ynam@kaist.ac.kr*

Abstract: Light-mediated neuromodulation techniques provide great advantages to investigate neuroscience due to its high spatial and temporal resolution. To generate a spatial pattern of neural activity, it is necessary to develop a system for patterned-light illumination to a specific area. Digital micromirror device (DMD) based patterned illumination system have been used for neuromodulation due to its simple configuration and design flexibility. In this paper, we developed a patterned near-infrared (NIR) illumination system for region specific photothermal manipulation of neural activity using NIR-sensitive plasmonic gold nanorods (GNRs). The proposed system had high power transmission efficiency for delivering power density up to 19 W/mm^2. We used a GNR-coated microelectrode array (MEA) to perform biological experiments using E18 rat hippocampal neurons and showed that it was possible to inhibit neural spiking activity of specific area in neural circuits with the patterned NIR illumination. This patterned NIR illumination system can serve as a promising neuromodulation tool to investigate neuroscience in a wide range of physiological and clinical applications.

OCIS codes: (180.0180) Microscopy; (260.3060) Infrared; (190.4870) Photothermal effects; (350.4238) Nanophotonics and photonic crystals; (330.5380) Physiology; (110.3960) Microlithography.

References and links

1. L. Fenno, O. Yizhar, and K. Deisseroth, "The development and application of optogenetics," Annu. Rev. Neurosci. **34**(1), 389–412 (2011).
2. V. Busskamp, S. Picaud, J. A. Sahel, and B. Roska, "Optogenetic therapy for retinitis pigmentosa," Gene Ther. **19**(2), 169–175 (2012).
3. D. Ghezzi, M. R. Antognazza, R. Maccarone, S. Bellani, E. Lanzarini, N. Martino, M. Mete, G. Pertile, S. Bisti, G. Lanzani, and F. Benfenati, "A polymer optoelectronic interface restores light sensitivity in blind rat retinas," Nat. Photonics **7**(5), 400–406 (2013).
4. L. Bareket, N. Waiskopf, D. Rand, G. Lubin, M. David-Pur, J. Ben-Dov, S. Roy, C. Eleftheriou, E. Sernagor, O. Cheshnovsky, U. Banin, and Y. Hanein, "Semiconductor nanorod-carbon nanotube biomimetic films for wire-free photostimulation of blind retinas," Nano Lett. **14**(11), 6685–6692 (2014).
5. D. Ghezzi, M. R. Antognazza, M. Dal Maschio, E. Lanzarini, F. Benfenati, and G. Lanzani, "A hybrid bioorganic interface for neuronal photoactivation," Nat. Commun. **2**, 166 (2011).
6. J. Suzurikawa, M. Nakao, Y. Jimbo, R. Kanzaki, and H. Takahashi, "Light-addressed stimulation under Ca(2+) imaging of cultured neurons," IEEE Trans. Biomed. Eng. **56**(11), 2660–2665 (2009).
7. J. Wells, C. Kao, K. Mariappan, J. Albea, E. D. Jansen, P. Konrad, and A. Mahadevan-Jansen, "Optical stimulation of neural tissue in vivo," Opt. Lett. **30**(5), 504–506 (2005).
8. A. R. Duke, M. W. Jenkins, H. Lu, J. M. McManus, H. J. Chiel, and E. D. Jansen, "Transient and selective suppression of neural activity with infrared light," Sci. Rep. **3**(1), 2600 (2013).
9. J. L. L. Carvalho-de-Souza, J. S. S. Treger, B. Dang, S. B. H. B. H. Kent, D. R. R. Pepperberg, and F. Bezanilla, "Photosensitivity of neurons enabled by cell-targeted gold nanoparticles," Neuron **86**(1), 207–217 (2015).
10. S. Yoo, S. Hong, Y. Choi, J.-H. Park, and Y. Nam, "Photothermal inhibition of neural activity with near-infrared-sensitive nanotransducers," ACS Nano **8**(8), 8040–8049 (2014).
11. P. Feyen, E. Colombo, D. Endeman, M. Nova, L. Laudato, N. Martino, M. R. Antognazza, G. Lanzani, F. Benfenati, and D. Ghezzi, "Light-evoked hyperpolarization and silencing of neurons by conjugated polymers," Sci. Rep. **6**(1), 22718 (2016).

#285594 https://doi.org/10.1364/BOE.8.002866
Journal © 2017 Received 26 Jan 2017; revised 5 Apr 2017; accepted 24 Apr 2017; published 4 May 2017

Biomedical Optics EXPRESS

12. N. Farah, A. Zoubi, S. Matar, L. Golan, A. Marom, C. R. Butson, I. Brosh, and S. Shoham, "Holographically patterned activation using photo-absorber induced neural-thermal stimulation," J. Neural Eng. **10**(5), 056004 (2013).
13. A. M. Leifer, C. Fang-Yen, M. Gershow, M. J. Alkema, and A. D. T. Samuel, "Optogenetic manipulation of neural activity in freely moving Caenorhabditis elegans," Nat. Methods **8**(2), 147–152 (2011).
14. F. Blumhagen, P. Zhu, J. Shum, Y.-P. Z. Schärer, E. Yaksi, K. Deisseroth, and R. W. Friedrich, "Neuronal filtering of multiplexed odour representations," Nature **479**(7374), 493–498 (2011).
15. S. Tsuda, M. Z. L. Kee, C. Cunha, J. Kim, P. Yan, L. M. Loew, and G. J. Augustine, "Probing the function of neuronal populations: combining micromirror-based optogenetic photostimulation with voltage-sensitive dye imaging," Neurosci. Res. **75**(1), 76–81 (2013).
16. X. Han and E. S. Boyden, "Multiple-color optical activation, silencing, and desynchronization of neural activity, with single-spike temporal resolution," PLoS One **2**(3), e299 (2007).
17. A. M. Packer, B. Roska, and M. Häusser, "Targeting neurons and photons for optogenetics," Nat. Neurosci. **16**(7), 805–815 (2013).
18. Y. M. Tamar Arens-Arad, N. Faraha, S. Ben-Yaishc, and A. Zlotnikc, "Head mounted DMD based projection system for natural and prosthetic visual stimulation in freely moving rats," Sci. Rep. **6**, 4–11 (2016).
19. K. Eom, J. Kim, J. M. Choi, T. Kang, J. W. Chang, K. M. Byun, S. B. Jun, and S. J. Kim, "Enhanced infrared neural stimulation using localized surface plasmon resonance of gold nanorods," Small **10**(19), 3853–3857 (2014).
20. S. Yoo, R. Kim, J.-H. Park, and Y. Nam, "Electro-Optical Neural Platform Integrated with Nanoplasmonic Inhibition Interface," ACS Nano **10**, 4274 (2016).
21. B. Nikoobakht and M. A. El-Sayed, "Preparation and Growth Mechanism of Gold Nanorods (NRs) Using Seed - Mediated Growth Method," Chem. Mater. **15**(10), 1957–1962 (2003).
22. P. Zhu, O. Fajardo, J. Shum, Y.-P. Zhang Schärer, and R. W. Friedrich, "High-resolution optical control of spatiotemporal neuronal activity patterns in zebrafish using a digital micromirror device," Nat. Protoc. **7**(7), 1410–1425 (2012).
23. N. Chakrova, B. Rieger, and S. Stallinga, "Development of a DMD-based fluorescence microscope," Proc. SPIE **9330**, 933008 (2015).
24. J. Jerome, R. C. Foehring, W. E. Armstrong, W. J. Spain, and D. H. Heck, "Parallel optical control of spatiotemporal neuronal spike activity using high-speed digital light processing," Front. Syst. Neurosci. **5**, 70 (2011).
25. T. A. Münch, R. A. da Silveira, S. Siegert, T. J. Viney, G. B. Awatramani, and B. Roska, "Approach sensitivity in the retina processed by a multifunctional neural circuit," Nat. Neurosci. **12**(10), 1308–1316 (2009).
26. S. Sakai, K. Ueno, T. Ishizuka, and H. Yawo, "Parallel and patterned optogenetic manipulation of neurons in the brain slice using a DMD-based projector," Neurosci. Res. **75**(1), 59–64 (2013).
27. N. Herzog, M. Shein-idelson, and Y. Hanein, "Optical validation of in vitro extra-cellular neuronal recordings," J. Neural Eng. **8**, 056008 (2011).

1. Introduction

Light-mediated neuromodulation techniques provide great advantages to investigate neural circuits due to its high spatial and temporal resolution. As an example, optogenetic technique modulates membrane potential by genetically modified light-sensitive ion channels. Its highly specified cell targeting ability, ion channel specificity and wavelength specificity open up various neuromodulation approaches from neurophysiology study to clinical trials [1,2]. In contrast, other neuromodulation techniques, which are free of genetic modification, have been developed using photovoltaic and photothermal mechanisms. Photoelectric methods stimulate neurons by generating photocurrents, and it has been reported that photovoltaic materials or photoconductive materials can be used to stimulate retinal ganglion cells [3,4] or cultured neurons [5,6]. Photothermal stimulation is a new method to modulate neural activity by generating heat locally at the periphery of the cell through external light and provide either excitatory or inhibitory stimulus to the cell. Irradiating infrared light, which generates heats to the surrounding medium for neurons, has been developed to excite [7] as well as inhibit [8] neural activity. To confine the effect of heat within more localized space, photothermal transducers were utilized. Plasmonic gold nanoparticles were used for its biocompatibility, controllability of plasmon wavelength, ease of surface functionalization and cell targeting capability [9,10]. Other small photo-absorbing materials such as microbeads or conjugate polymer were also demonstrated to modulate neural activity [11,12].

To control spatial pattern of neural activity, it is necessary to generate patterned-light illumination to the specimen. To this end, a digital micro-mirror device (DMD) has been used

Biomedical Optics EXPRESS

in various neurophotonic instrumentation due to its simple configuration and design flexibility. In optogenetic applications, DMD was used to target specific neurons in freely moving C-elegans [13], to generate odor patterns in the olfactory bulb of zebra fish [14], and to analyze inhibitory circuit in the mouse cerebellar cortex [15]. In other studies, it was used to apply photocurrents only to the desired neurons cultured on photovoltaic polymer [5] or photoconductive material [6]. In these applications, low power density (0.2 ~18 mW/mm^2) was sufficient to activate light-induced changes in optogenetics [16,17], photovoltaic [5,18] and photoconductive [6] effects. In photothermal modulation, however, the relatively high power density of visible or infrared light is needed to manipulate neural activity through either excitation or inhibition. Intense power density (10 W/mm^2 ~10 kW/mm^2) with ultrashort pulse width was required for neural excitation [9,19], while moderate power density (10 mW/mm^2 ~30 mW/mm^2) with prolonged pulse width was used for neural inhibition [10,11,20]. Despite the promising capability of photothermal methods, spatial patterning of photothermal illumination has not been investigated.

Here we report the implementation of a power efficient spatial light stimulation system for near-infrared photothermal neural modulation technique. Plasmonic photothermal neuromodulation technique converts light into heat through plasmonic metal nanoparticles that are in close proximity to the cell membrane. We used DMD to generate near-infrared spatial light patterns and surface-immobilized gold-nanorods array to convert the light patterns into thermal patterns. The main focus of the system was to produce spatially uniform power intensity over the illumination area while minimizing the optical power loss from the light source to the specimen. As the photothermal methods require high power density (10 ~10 kW/mm^2), it is desired to have minimal power loss in optical components. At the same time, the spatial uniformity of the optical power density is also required. To meet these requirements, we projected a circular multimode fiber tip image to DMD surface and relayed the DMD patterns to the sample surface while minimizing the number of the optical components. We carefully characterized the power transmission of the light path and maximum pattern resolution. Then, we validated that temperature pattern was localized at the illumination pattern using GNR coated glass substrate. Finally, we demonstrated localized neural suppression using cultured hippocampal neurons.

2. System design for patterned illumination

Figure 1 shows overall system diagram and optical pathways of patterned NIR illumination. NIR light from a commercialized laser module (450 mW maximum power, continuous wave 785 nm diode laser, B&W Tek) was illuminated to a DMD (DLP3000FQB, Texas Instruments) through an aspheric lens (C240TME-B, NA = 0.5, f = 8 mm, Thorlabs) and a mirror (BB1-E03, Thorlabs). Then, patterned light by DMD was delivered to a sample substrate through optical components in a microscope system. This system can be divided into four components: (1) optical components for uniform pattern intensity, (2) DMD for spatial light pattern, (3) GUI interface program to control the DMD and (4) a microscope system to deliver the light pattern to sample substrate.

To avoid illumination vignette, we designed the optical components to illuminate DMD with uniform light intensity. We utilized a multimode fiber that has uniform spatial power distribution at the tip. Magnified circular pattern at the fiber tip (NA = 0.22, 105 μm diameter) was projected to DMD surface using an aspheric lens, a mirror, and micromanipulators. To transfer the highest power density available, positions of the aspheric lens and fiber tip were adjusted to locate the magnified core pattern to be at the height of the DMD (3.7 mm tall).

To shape illumination pattern, a commercialized DMD (DLP3000FQB, Texas Instruments) with its evaluation board (DLP® LightCrafter Evaluation Module, Texas Instruments) was used with its LED light engine eliminated. This compact, inexpensive DLP module includes DMD that has sufficient reflectance range from visible to NIR. The DMD was placed at the focal plane of a tube lens (f = 180 mm) where a CCD camera is typically

Biomedical Optics EXPRESS

located in conventional microscope setups. The position of DMD and the angle of incident light to DMD were precisely adjusted to guide the reflected light pattern to a microscope frame (IX73, Olympus) through the center of optical components.

MATLAB (Mathworks Inc.) based GUI program was designed to interface with DLP module that controls pixels in DMD. In addition to the control, the GUI program was designed to properly modify the resolution of input image patterns such that the DMD can correctly project the patterned illumination to the sample. Because of the unequal width (5.4 μm) and height (10.8 μm) of the DMD pixels, the projected image from 604 x 684 pixels becomes WVGA resolution image (854 x 480 pixels). Thus, we loaded input images in WVGA resolution to the GUI program and had the program scale the images to the DMD pixel resolution (604 x 684 pixels) using nearest neighbor interpolation. Then, the transformed images were transferred to the DLP module for projection with WVGA resolution to the sample substrate.

The light pattern reflected from DMD was transferred into the microscope frame and projected to the sample substrate using a bright field objective lens with various magnification. To avoid pattern distortion, objective lenses without phase ring were used (4X: UPlanFLN, 10X: UPLSAPO10X2, Olympus). For design flexibility toward simultaneous multiple optical recordings in different wavelength ranges, objective lenses that have sufficient transmittance (> 80%) in the visible range and NIR range were used. For higher pattern resolution, water immersion lenses were used (20X, 40X, UMPLFLN, Olympus). Numerical aperture was 0.13, 0.4, 0.5 and 0.8 for 4X, 10X, 20X and 40X respectively.

We observed the illuminated light pattern that was reflected from the sample substrate through a beam splitter (21000, Chroma Technologies Corp), a low side C-mount with internal tube lens (IX3-RSPC, Olympus) and an EMCCD camera (Luca, ANDOR). This image provides valuable feedback to align optical components. For alignment, 400 nm thick gold film coated glass substrate was used with water immersion lenses for the highest illumination resolution.

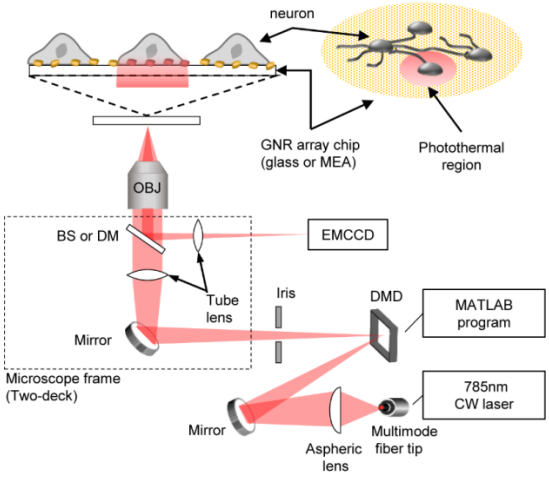

Fig. 1. Diagram of the patterned illumination system. This system consists of NIR laser source, reflective mirror, DMD, MATLAB-based GUI program, microscope frame, beam splitter (BS), dichroic mirror (DM) and objective lens (OBJ). The GNR array chip was used for converting plasmonic photothermal stimulation.

3. Methods and materials

3.1 Measurement of power uniformity

To measure spatial profile of the entire illumination pattern, we measured the light power delivered from each portion of DMD area and combined the results. We divided the whole

Biomedical Optics EXPRESS

DMD pixel area (6.57 × 3.69 mm^2) into 9 x 16 of small non-overlapping pixel areas (380 × 380 μm^2) as in Fig. 2(a), (top). Then the power of each pixel area was measured by power meter (XLP12-3S-H2, Gentec-EO, Québec, CA). To illuminate the finest pattern, we used the water immersion objective lens (20X) of high NA (0.5) with water filled between the sample and the objective lens.

3.2 Minimum illumination linewidth test

To investigate the minimum linewidth our illumination system can project, we projected various line patterns with different width and measured the intensity profile. Binary images with different line width (1, 2, 5 and 10 lines) in DMD active pixel resolution (604 × 684 pixels) were designed and projected to the substrate. Then, the intensity profile perpendicular to the projected line was measured, and the maximum intensity in that profile was compared to that of the whole illumination to find out the minimum number of pixel lines required to illuminate the same intensity. For the finest illumination, we used high NA objective lens (20X, 0.5). It is also possible to measure the intensity profile of illuminated pattern using current Andor EMCCD because pixel density of imaging system (1004 × 1002 pixels / per 6.58 × 4.96 mm) was higher than that of the illumination system (604 × 684 pixels / per 6.57 × 3.69 mm). There was no binning during image acquisition.

3.3 Fluorescence thermal imaging

We used fluorescence dye Tris(2.2'-bipyridyl-d8) ruthenium (II) hexafluorophosphate (Sigma-Aldrich, #652407) due to its high linearity at wide temperature range and high thermal quenching coefficient [12]. The dye was diluted in 1:1 mixture of DMSO and water to 0.8 nM for strong fluorescence signal and the dye solution (20 μl) was sandwiched between GNR coated glass and coverslip to measure 2D temperature profile. The height of the dye layer was estimated to be 4 μm, which was calculated by dividing total volume of dye to the surface area of coverglass. We applied 470 nm LED light (M470L3-C1, Thorlabs) to excite the dye molecules. Emission light was delivered to the camera through two dichroic mirrors (DM1: 505 nm, DM2: 770 nm cutoff, Olympus), and an emission filter (575~625 nm, Chroma). All chromatically corrected objective lenses used here exhibit a transmittance of more than 90% over the range of 470 to 675 nm and a transmittance of at least 75% for the 785 nm wavelength. To reduce photo bleaching, the intensity of excitation light was kept minimized and exposure time was synchronized to the fire signal of EMCCD. Fluorescence image was acquired using EMCCD (bining: 2 × 2, frame rate: 17 Hz).

To obtain the calibration curve between temperature and fluorescence intensity change, the GNR coated glass coverslip (Borosilicate glass D 263®, 01111580, Paul Marienfeld GmbH & Co. KG, Germany) was set to several temperatures in the range of interest (30 ~48 °C) with 5-min of settling period and the fluorescence intensity (ROI area: 600 x 600 μm^2, 4X lens) was sampled with a brief exposure (30 ms). The temperature of the glass coverslip was controlled by a heating plate (TC01, MultiChannel Systems) which had the feedback thermal sensor underneath the plate. To minimize any systematic measurement error due to the photobleaching, each exposure time was kept short (30 ms) and the temperature measurement was carried out 2 ~3 times in random order. The fluorescence intensity of 37 °C was used as the reference value.

To measure the temperature changes for different illumination conditions (illumination area: 1.09 mm^2, 0.0436 mm^2, 0.0109 mm^2 for 4X, 20X, 40X, respectively), three trials (each trial 30 sec) were collected. To calculate spatial thermal profile, fluorescence intensity signal from each pixel of the image was measured during 12 trials (10 s illumination with 20 s interval). To compensate any photobleaching effect, each trial was normalized by the corresponding baseline value (average of 5 s before illumination) and averaged. Then the temperature was calculated using the calibrated relationship between temperature and fluorescence intensity. Thermal profile was smoothened by the median filter (5 × 5 pixels) for

Biomedical Optics EXPRESS

visual clarification. Despite low NIR transmittance of emission filter, reflected NIR light added the baseline offset value by 1% for the 4X lens. To calculate the temperature change, the corrected fluorescence intensity values were used. In the case of 20X and 40X, the baseline offset was insignificant.

3.4 GNR synthesis

GNR was synthesized by seed-mediated method [21]. Briefly, seeds were synthesized by mixing the following chemicals: 1 mL of 0.2 M cetyltrimethylammonium bromide (CTAB, Sigma), 1 mL of 0.5 mM $HAuCl_4$ (Sigma), and 120 μL of 0.01 M $NaBH_4$ (Sigma). The seed was elongated to rod shape in the mixture of following chemicals: 5 mL of 0.2 M CTAB, 5 mL of 1 mM $HAuCl_4$, 250 μL of 4 mM $AgNO_3$ and 70 μL of 78.84 mM ascorbic acid. The synthesized gold nanorod was purified by centrifuge (10,000 rpm, 10 m) and resuspended in deionized water. The gold nanorods(GNRs) were functionalized by SH-PEG(5 k)-NH_2 (Nanocs, MA, USA) for biocompatibility and substrate binding. GNRs showed absorption peak (800 nm) at NIR region (785~800 nm), and zeta potential was + 20 mV.

3.5 Substrate coating with GNRs

GNRs were deposited on the culture substrate (glass coverslip or MEA) using a previously reported method [20]. Before the integration of GNR, bare substrate was cleaned with acetone, isopropyl alcohol (IPA) and DI water in an ultrasound bath for 5 min respectively. The substrate was functionalized by air plasma (1 min), and the suspension of positively charged GNR-PEG-NH_2 (1 optical density) was applied to the substrate for 12 hours in a humidified incubator (37 °C, 5% CO_2). After the incubation, the supernatant was removed, and the coated substrate was rinsed with DI water twice. The absorption peak of the GNR-coated chip was 820 nm, which was slightly red-shifted by 20 nm from that of the GNR suspension (800 nm). Normalized optical density at the excitation wavelength (785 nm) was 0.88.

3.6 Cell culture

Before cell seeding, the GNR-coated MEA substrates were coated with poly-D-lysine (PDL, 0.1 mg/mL in Trizma buffer pH 8.5, Sigma) for 3 hours for improved cell adhesion and neurite outgrowth. Then, these substrates were sterilized by 70% ethanol and fully dried in a laminar flow hood. Hippocampi were dissected from E18 Sprague–Dawley rat (Koatech, Korea), mechanically dissociated in Hank's balanced salt solution (HBSS, WelGENE, Korea). Cells were collected by centrifuge at 1000 rpm for 2 min, and the supernatant was removed. The pallet was resuspended in a plating medium of Neurobasal medium supplemented with B27 (2%, Invitrogen), glutamax (2 mM, Invitrogen), glutamate (12.5 μM, Sigma), and penicillin–streptomycin (1%, Invitrogen). Cells were plated on MEA at target density (800 cells/mm^2) on a small area covering electrodes. The neural culture was maintained in an incubator (5% CO_2 and 37 °C), and half of medium was replaced every 5 days with fresh culture medium (plating medium excluding glutamate). All experiments were performed in accordance with the guidance of the Institutional Animal Care and Use Committee (IACUC) of Korea Advanced Institute of Science and Technology (KAIST), and all experimental protocols were approved by IACUC of KAIST.

3.7 Neural recording and data processing

We used commercial MEA chips as the culture substrate (60MEA200/30iT-ITO, Multichannel Systems, Germany), which consist of 1 internal large ground electrode and 59 titanium nitride (TiN) microelectrodes (30 μm and 200 μm spacing of grid pattern) with transparent indium tin oxide (ITO) connection lines. A custom-made neural amplifier was used to record neural activity from extracellular electrodes (1000 V/V, 150~4500 Hz). The amplifier output was digitized by MC Card (12 bit, 25 kS/s, Multichannel systems) and then

Biomedical Optics EXPRESS

high-pass filtered by a second order Butter-worth filter (f_c = 200 Hz) in MC_Rack program (Multi Channel Systems). To quantify the degree of neural suppression, we extracted neural spikes using thresholding method (threshold = - 6 × standard deviation of background noise). To prevent any laser-switching artifact from being counted as spikes, spikes detected within 10 ms-window at the onset and offset of the laser (± 10 ms) were ignored using NeuroExplorer (Nex technologies, USA). Then, the spike rate change was measured by comparing spike rate during and before illumination for the same period (10 s). The 10 sec illumination period was used to reliably estimate the change of spontaneous spike rates that ranged from 0.1 Hz to 10 Hz.

4. Results

4.1 Spatial power density in effective pixel area

To investigate the uniformity of illuminated pattern we measured the effective uniform power density pixel area of DMD. First, we verified that all optical compartments (fiber tip, DMD, and camera) were well positioned at the image plane. Figure 2(a), (top) shows reflected fiber tip pattern from sample substrate when all DMD pixels were activated. Through clear circular magnified fiber tip pattern and clear truncated area that shows DMD pattern in this figure, we confirmed good alignment of the optical components. We also confirmed that the circular fiber tip pattern was magnified by 50 times from its EMCCD image whose diameter was 5.2 mm.

Next, the spatial power profile was characterized. The power of light reflected from each small square DMD area in Fig. 2(a), (top) was measured for every component (9 × 16) and displayed as a contour plot in Fig. 2(a), (bottom). This power density map shows “top hat” profile that is required for this system. We then characterized the effective pixel area within which the power density is uniform. Figure 2(b) shows normalized power profiles from 4, 5 and 6th row of spatial power density map including an averaged one. It was found that the effective pixel area was the circular area with the diameter of 4.3 mm defined by the full-width half maximum of the profile in Fig. 2(b).

4.2 Power transmission efficiency

We investigated the efficiency in the transmission of light by characterizing power loss at each system node by a power meter (Fig. 2(c)). Under 100% laser output (450 mW), the amount of light that reached the sample stage from the laser source was 25%. There was 60% loss at DMD and 20% loss at the objective lens (Fig. 2(d)). The power loss at other optical components was negligible (< 3%). We could achieve higher power density with higher magnification lens at the cost of the smaller addressable area. In this configuration, 4.3 mm diameter of DMD pattern corresponded to the addressable area of 860, 330, 165 and 80 μm diameter for 4X, 10X, 20X and 40X magnifications, respectively. The achievable maximum power density was 0.1, 0.9, 3.7 and 19 W/mm^2 for 4X, 10X, 20X and 40X magnifications, respectively.

Biomedical Optics EXPRESS

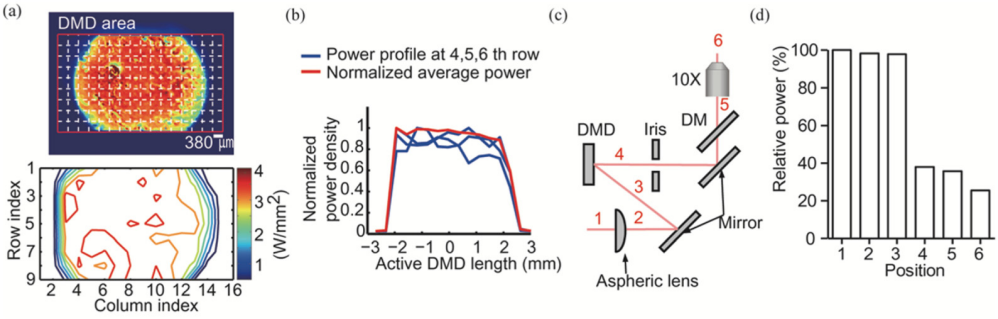

Fig. 2. Characterization of the effective pixel area and power transmittance. (a) Reflected illumination pattern from sample substrate. Magnified circular fiber tip image truncated by DMD height limit is presented in CCD field of view (top). The outer red square indicates DMD area and inner white squares indicates unit areas for power measurement. Spatial power profile measured from (a) in 9 x 16 resolution by scanning method (bottom). The scale bar, calculated by 20X image, shows the width of measurement unit (380 × 380 μm^2) in actual DMD. (b) One dimensional profile of normalized power density of three rows in the middle of power profile (blue) and averaged one (red). The measurement was obtained by 20X water immersion lens with high NA (0.5). (c) Simplified beam path with optical components that transfer or reflect light. In all case, beam size was smaller than sensor area of the power meter. (d) The relative power of each position in (c).

4.3 Minimum resolution of illumination

To characterize the smallest pattern this system can reliably generate, we investigated the minimum line width of vertical and horizontal patterns under the specific illumination condition (20X). Although minimum optical linewidth is decided by the magnitude and NA of the objective lens, we need to know how many lines in active DMD should be turned on together to make a line pattern of maximum light intensity (i.e. the same power level as in the whole illumination). Figures 3(a), (b); (top) shows reflected binary pattern images from sample substrate with different linewidth (1, 2, 5 and 10 pixels) in DMD active pixel resolution (604 × 684 pixels). These line width values correspond to 10.8, 21.6, 54 and 108 μm horizontally and 5.4, 10.8, 27 and 54 μm vertically right on the DMD area. The width of projected lines to the sample is 20 times smaller with the 20X lens. The intensity profile perpendicular to projected line was measured (i.e along the red dotted lines in Figs. 3(a), (b) (top) and maximum intensity in that profile was compared to that of the whole illumination to find out the minimum number of pixel lines required to illuminate the same intensity. We found that at least 5 vertical lines and 10 horizontal lines should be recruited for the same maximum intensity as the whole illumination (Figs. 3(a) ,(b) (bottom). Two times difference between vertical and horizontal lines was due to the fact that the number of DMD pixels needed for a single vertical line is two times more than that for a single horizontal line. Thus, the smallest unit with maximum power density was 10 pixels long and 5 pixels wide. Based on the size of DMD pixels, this smallest unit theoretically corresponded to 2.7 μm in both horizontal and vertical directions on the sample when the 20X lens was used. Calculated smallest unit size by full width half maximum in Fig. 3 was 2.5 μm, similar to the theoretical value. Figure 3(c) shows various NIR patterns that could be readily projected on a microelectrode array.

Biomedical Optics EXPRESS

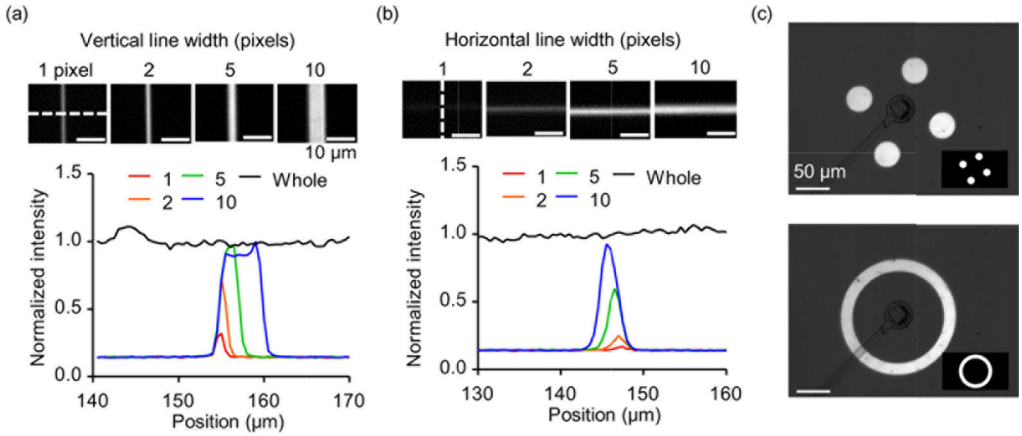

Fig. 3. The spatial line width of 20X magnification condition. Reflected illumination line pattern substrate: vertical lines (a, top), horizontal lines (b, top). The intensity profile of red line from the upper figure for different vertical line width (a, bottom) and horizontal line width (b, bottom). Intensity profile was normalized by the mean value of intensity in the case of whole pixel activation from 140~170 μm (vertical) and 130-160 μm (horizontal). (c) Reflected images of various NIR patterns (four-circles (top), donut (bottom)) under low intensity background illumination (Inset: binary mask patterns).

4.4 Measurement of patterned photothermal effect

Figure 4(a) describes how we measured the temperature of GNR coated substrate under NIR illumination. As the patterned NIR illumination was to generate heat pattern for localized neural suppression, we examined the temperature change and the thermal profile in the confined illumination area. Figure 4(b) shows the calibration curve for the sensor dye that we used in this study. Linear regression shows that temperature-intensity relationship was estimated to –0.84%/ °C with good fitting quality (R-square: 0.98). Based on the linear relationship, the temporal dynamics of temperature change in GNR coated substrate was estimated. Figure 4(c) shows three different temperature measurement for different objective lenses. With the whole DMD pixels activated, temperature changes were 10.6, 5.6 and 4.4 °C with 40X, 20X and 4X lenses under 2124, 492 and 28 mW/mm^2. We could obtain the sufficient temperature increase (8 ~10 °C) that is needed to completely suppress the neural activity of spiking neurons [20]. Next, we tested the co-localization of heat pattern and light pattern. With 20X objective lens, 70 μm circle was illuminated with the power density of 456 mW/mm^2. Figure 4(d) and (e) shows the measured heat pattern before and during the patterned illumination. Before the illumination, there was no heat pattern (Fig. 4(d), red dashed circle), while it was observed that there was significant temperature change at the circled region during the illumination.

Biomedical Optics EXPRESS

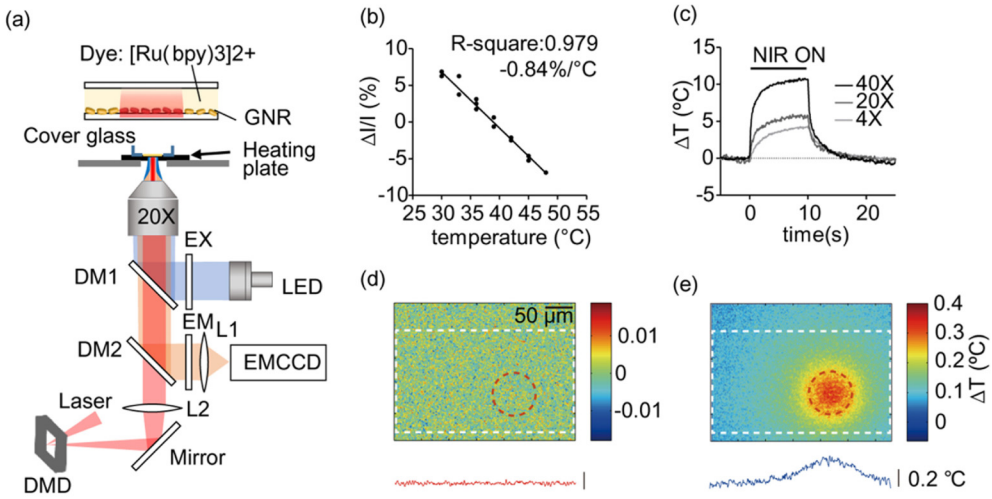

Fig. 4. Fluorescence thermal imaging of GNR coated substrate. (a) The experimental diagram to measure fluorescence intensity during patterned illumination. Dichroic mirror; DM, excitation filter; EX, emission filter; EM, tube lens; L. (DM1: 505 nm, DM2: 770 nm cut off, EX: 420-460 nm, EM: 575-624 nm, 3OD@785 nm). (b) The relationship between temperature and normalized fluorescence intensity change. (c) Calculated temperature dynamics from three different illumination condition (4X, 20X, 40X). For each magnification, three trials were normalized by pre-illumination value and averaged. Despite low NIR transmittance of emission filter (3 OD), reflected NIR pattern was captured during fluorescence imaging, which results in a slight offset in calculated temperature (4X result). (d-e) Spatial heat profile for the non-illumination period (before 5 s) (d) and during illumination (5 s after laser on) (e). The white square indicates DMD area and the red circle indicates a pattern (70 μm diameter) that is projected using 20X water immersion lens. The power density of pattern was 456 mW/mm^2. The images were averaged over 12 trials and smoothened for visual clarification using 5 × 5 median filter.

4.5 Area specific neural suppression with patterned illumination

With the optimized system and conditions above, we attempted to modulate the firing rate of specific neurons illuminated by photothermal patterns. We tried to induce local inhibition effect under patterned illumination using a GNR-coated MEA that was effective in suppressing neural activity [20]. Cultured hippocampal neurons on a GNR-coated MEA was used for simultaneous optical modulation and neural recording. Circular light pattern, whose center was located on a single electrode (Ch 13) with various diameter values (360, 540, 720 and 900 μm), was illuminated with a moderate power level (35 mW/mm^2) (Fig. 5(a)) and the suppression effect on the illuminated region versus non-illuminated region was compared through the electrodes located inside and outside the illumination region.

In all illumination sizes, area specific suppression effect was observed. Figure 5(b) shows the actual illuminated pattern on the MEA, and Fig. 5(c) shows neural signals from the electrode at the center of the illumination region, at 560 μm apart, and 1 mm apart from the center electrode. When the circular pattern was 360 μm, the suppression only occurred inside the pattern. As the illumination size increased from 360 μm to 900 μm, the neural activity decreased from 62% to 97% in the illumination area (Ch 13). In contrast, there was no suppression effect for very distal part (1 mm apart, Ch 64). In the case of the neural activity in the vicinity of the pattern (565 μm apart from the pattern center, Ch 35), the significant suppression appeared when the illumination pattern approach near the electrode. This indicated that we could create local suppression through our NIR-DMD system and the degree of suppression could be controlled by the pattern size. Figure 5(d) shows the spike rate change during the 10-second NIR illumination period with respect to the baseline activity.

Biomedical Optics EXPRESS

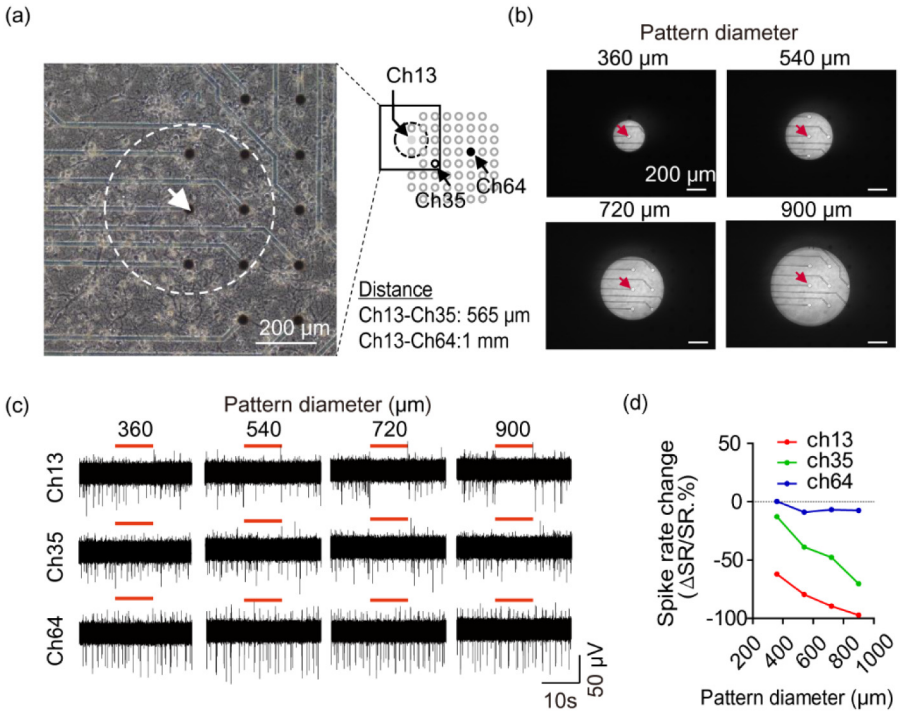

Fig. 5. Area specific neural suppression. (a) Phase contrast image of a cultured hippocampal neuronal network on a GNR-coated MEA. White arrow and dashed line show recording electrode (ch13) and illumination area, respectively. The location of three electrodes (ch13, ch35, and ch64) are marked in the electrode layout (right). (b) Reflected image from MEA under illumination of a different pattern whose center is ch13 (arrow) under 4X magnification. (c) Simultaneous neural recording from three electrodes (ch13, ch35, and ch64) for different illumination pattern diameter. (d) Spike rate change of ch13, ch35, and ch64 during for different illumination diameters. Power density was 35 mW/mm2.

4.6 Application to light-induced electrical noise elimination

To demonstrate the versatility of our system, we attempted to remove the light-induced electrical noise by illuminating the light pattern that masks the electrode area. Figure 6 shows microelectrode recordings with and without the optical electrode mask. When a 165 μm-diameter circular area centered at the electrode was illuminated with 970 mW/mm^2 (Fig. 6(i)), there was a large electrical noise during the high power light illumination, which severely interfered with the monitoring of neural spikes due to the increased noise level (2.34 μV_{rms} to 5.27 μV_{rms}). Based on the assumption that the electrical noises could be the NIR-induced thermal noise at the TiN microelectrode, a small circle was added to the DMD illumination pattern to mask the electrode area (Fig. 6(ii)). In this case, there was no noise increase during the illumination period and only the light-induced switching artifact at the onset and offset of the laser was present. Thus, it was confirmed that the spiking activity that was present before the illumination was suppressed during the high-power NIR illumination and the activity was recovered after the illumination. Without the electrode masking, it could not have been confirmed through the electrode recording.

Biomedical Optics EXPRESS

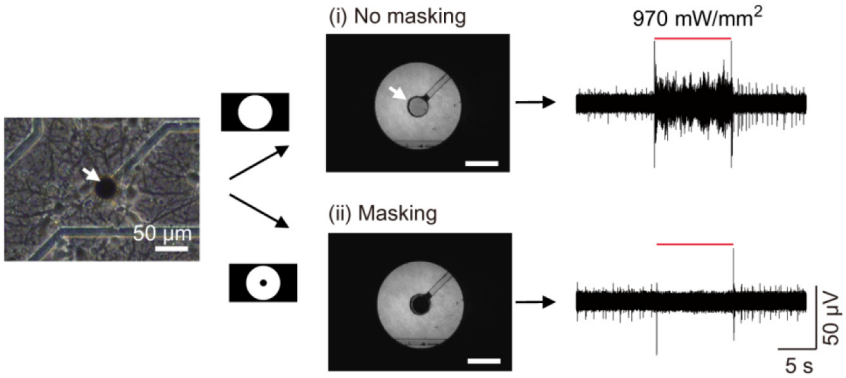

Fig. 6. Prevention of light-induced artifact for photothermal neural inhibition experiment. (a) Neural spike recording under the circular illumination (165 µm diameter) including a recording TiN (30 µm diameter, white arrow). Light-induced noise artifact is shown during the illumination. (b) Artifact-free neural spike recording with the electrode mask pattern. Objective lens: 20X. The red bar shows the illumination period.

5. Discussion

For the first time, we developed DMD-based patterned NIR illumination and successfully demonstrated localized inhibition of neural activity using a GNR-coated MEA under patterned NIR illumination. So far, only one neuromodulation study with patterned NIR was reported using two-photon scanning system [12]. In the case of the scanning system, the design flexibility of the spatial light pattern is lower than the DMD system, and maximum power density is limited by illumination area. Moreover, our system showed uniform pattern intensity with simple optical components. Several optical configurations have been implemented as light pattern generator to avoid illumination vignette. Expanded collimation [22], diffuser [23] and beam shaper [24] have been used for light homogenization, but severe power loss limits maximum applicable power density. Fly eye lens makes flat illumination by dividing each spatial beam path, but the lens dimension should be customized to guide light pattern into a microscope. Due to the complexity of illumination system with fly eye lens, several pattern illumination systems combined microscope to commercialized beam projector equipped with fly eye lens [18,25,26]. In our work, only one aspheric lens with multimode optical fiber makes the system very simple with minimizing power loss only at the cost of lower usable DMD area. And, we were able to achieve high power transmittance (30%) compared to previously reported works (< 10%) [15,22].

We showed that the firing rate of a neuron could be controlled by changing the illumination pattern size. As shown in Fig. 5(d), the suppression level increased monotonically as the pattern size increased. Considering that an electrode captures neural activity from cells within close distance (60 µm) [27], adjusting the diameter of circular illumination pattern might be controlling the number of neurons that influence the recording neuron. The inhibition was also dependent upon the distance from the illumination area, which made it possible to obtain area-specific neural inhibition. The area specificity also depended on the pattern size and the distance from the pattern. If it was too far from the illumination area (Ch 64, Fig. 5(d)), the inhibition did not occur at all. The illumination size is not the only variable that can control the inhibition. The neural suppression can be also controlled by the illumination intensity. According to our previous studies based on a wide-field illumination (size: 5 mm in diameter) [10,20], firing rates of spiking neurons could be regulated through the laser intensity control. Although it was not explicitly demonstrated in this work, it is expected that the inhibition level would be also be controlled by the intensity control with our DMD system, which could give us several control variables (size, distance and intensity) for neural inhibition.

Biomedical Optics EXPRESS

The spatiotemporal resolution of neural inhibition is not limited to the presented results. Although most of the patterns were much larger than a single cell scale (10 ~30 μm in diameter), it was hinted in Fig. 6 that smaller illumination sizes would be possible with higher power density. Comparing with the power level and the pattern size, much higher power density (35 vs. 970 mW/mm^2) was needed to inhibit neural activity as the illumination size was reduced by the factor of 5.5 (900 μm vs 165 μm). If the pattern size reduces to a 20 μm size spot, a few tens of W/mm^2 is expected to be needed, which could be readily achieved by replacing our laser source (max. 450 mW) with a higher power laser source (1 ~4 W). Concerning the temporal resolution of the neural inhibition, we used 10-sec duration which was in our previous studies [10,20]. But this does not imply that the 10 second duration is minimum time for the suppression. In our previous study, it was shown that the time scale of neural inhibition was on the order of a few hundred milliseconds under the illumination size of 5-mm diameter [10]. Feyen et al. used 500 ms light pulse to show the suppression of action potential from primary hippocampal neurons [11]. Thus, the time scale of the neural inhibition should be much shorter than the pulse duration of 10-second, and its limitation at the cellular scale is yet to be investigated. It is worthwhile to note that the millisecond range neural responses have been reported with 1-ms or sub-millisecond light pulses in photothermal neural excitation studies [9,12].

6. Conclusion

In summary, we developed a DMD based NIR patterned illumination system for plasmonic photothermal neuromodulation. Two important features were obtained from our design: a uniform power intensity in the field-of-view and low-loss power transmission. Based on these features, the maximum power density of 19 W/mm^2 were achieved for the addressable area of 80 μm in diameter. Using a nanoplasmonic photothermal platform based on gold nanorods, it was confirmed that local area specific neural suppression in hippocampal neural networks was possible. We further demonstrated that our DMD system could be applied to overcome the light-induced electrical noise interference problem in electrophysiological experiments. The application of patterned inhibition to currently existing in vitro culture system may provide insight to further understand the neural system. We believe that the selective neural suppression platform can serve as a promising neuromodulation tool for neuroscience in a wide range of physiological and clinical applications.

Funding

Basic Science Research Program through the National Research Foundation of Korea (NRF) funded by the Ministry of Science, ICT and Future Planning (NRF-2015R1A2A1A09003605).